University of New Orleans

# ScholarWorks@UNO

Electrical Engineering Faculty Publications

Department of Electrical Engineering

# Polarizing properties of embedded symmetric trilayer stacks under conditions of frustrated total internal reflection

Rasheed M.A. Azzam
*University of New Orleans*, razzam@uno.edu

Siva R. Perla

### Recommended Citation

Rasheed M. A. Azzam and Siva R. Perla, "Polarizing properties of embedded symmetric trilayer stacks under conditions of frustrated total internal reflection," Appl. Opt. 45, 1650-1656 (2006)

# Polarizing properties of embedded symmetric trilayer stacks under conditions of frustrated total internal reflection

Rasheed M. A. Azzam and Siva R. Perla

An all-transparent symmetric trilayer structure, which consists of a high-index center layer coated on both sides by a low-index film and embedded in a high-index prism, can function as an efficient polarizer or polarizing beam splitter under conditions of frustrated total internal reflection over a wide range of incidence angles. For a given set of refractive indices, all possible solutions for the thicknesses of the layers that suppress the reflection of either the $p$ or $s$ polarization at a specified angle, as well as the reflectance of the system for the orthogonal polarization, are determined. A 633 nm design that uses a $MgF_2$–$ZnS$–$MgF_2$ trilayer embedded in a ZnS prism achieves an extinction ratio (ER) > 40 dB from 50° to 80° in reflection and an ER > 20 dB from 58° to 80° in transmission. IR polarizers that use $CaF_2$–$Ge$–$CaF_2$ trilayers embedded in a ZnS prism are also considered. © 2006 Optical Society of America

*OCIS codes:* 230.5440, 240.0310, 260.5430, 310.0310.

## 1. Introduction

Thin-film polarizers and polarizing beam splitters (PBS) are widely known[1–4] and are based on the destructive interference of light for one linear polarization ($p$ or $s$) and the nearly full constructive interference for the orthogonal polarization.

In this paper we consider the polarizing properties of a symmetric trilayer stack of refractive indices $n_1$, $n_2$, $n_1$, which is embedded in a high-index medium (prism) of refractive index $n_0$; see Fig. 1. All media are considered to be transparent, optically isotropic, and separated by parallel-plane boundaries. We also assume that $n_0 > n_1$, $n_2 \geq n_0$ and that light is incident from medium 0 at an angle $\phi_0$, which is greater than the critical angle [$\phi_{c01} = \arcsin(n_1/n_0)$] of the 01 interface, so that frustrated total internal reflection (FTIR) takes place.

In a recent paper[5] Li and Dobrowolski reviewed the earlier literature about polarizers that employ FTIR and proposed a new high-performance PBS that reflects the $p$ polarization and transmits the $s$ polariza-tion. (In the conventional MacNeille design[6,7] that operates at Brewster's angle, the $p$ polarization is transmitted and the $s$ polarization is reflected.) The Li and Dobrowolski design uses a symmetric trilayer (3) of thin films as a basic unit (period), which is repeated many times (9–27). Therefore the full multilayer consists of as many as 81 thin films.

In Section 2 we consider polarizers that consist of only one period (trilayer), and we do not resort to the thin-film approximation of Ref. 5. Also, instead of using Herpin's equivalent-layer theory,[8,9] we introduce an explicit technique that is based on the full expressions of the complex-amplitude reflection coefficients of the trilayer structure. We also allow for either the $p$ or $s$ polarization to be reflected or transmitted.

In Section 3 we assume a set of refractive indices, and we determine all possible embedded symmetric trilayers that suppress the reflection of $p$- or $s$-polarized light at each one of several angles of incidence $\phi_0$, while boosting the reflection of the orthogonal polarization toward 100%. We find a continuum of solutions at each angle and for each polarization. Results are presented for visible-laser (633 nm) polarizers that use $MgF_2$–$ZnS$–$MgF_2$ trilayers embedded in a Cleartran[10] (ZnS) prism.

In Section 4 a specific trilayer stack is described that functions as a dual polarizer (or PBS) at two widely separated angles of choice (e.g., 55° and 75°).
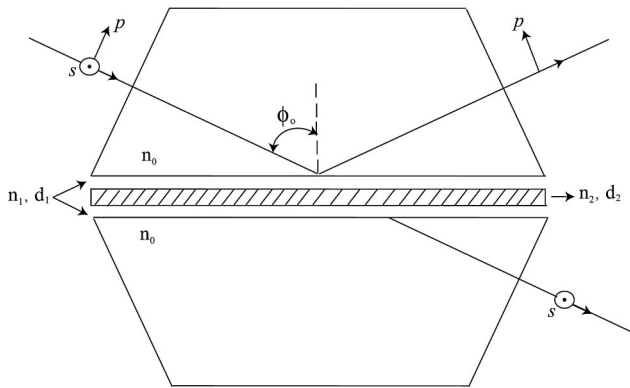
Fig. 1. Embedded trilayer structure as a polarizing beam splitter (PBS). A PBS in which the $p$ polarization is transmitted and the $s$ polarization is reflected is also considered. See text for discussion.

One such $MgF_2$–$ZnS$–$MgF_2$ trilayer embedded in a Cleartran (ZnS) prism achieves an extinction ratio in reflection $ER_r > 40$ dB over the 50°–80° angular range and an extinction ratio in transmission $ER_t > 20$ dB over the 58°–80° range. The angular range measured in air outside the prism is even larger if one accounts for refraction at the entrance face of the prism by using Snell's law. The response of this wide-angle design to a 600–700 nm spectral scan is also considered.

In Section 5 we present results for infrared polarizers that use the $CaF_2$–$Ge$–$CaF_2$ trilayer embedded in a ZnS prism. Finally, Section 6 gives a brief summary of the paper.

## 2. Design Procedure

Consider a monochromatic light beam traveling in an ambient medium (solid prism) of refractive index $n_0$ and incident on an embedded symmetric trilayer structure at an angle of incidence $\phi_0$ with respect to the normal to the interfaces, as shown in Fig. 1. The overall complex-amplitude reflection coefficient for $v$-polarized light ($v = p$ or $s$) can be expressed as[11]

$$r_v = \frac{l + mX_1 + nX_2 - mX_1 X_2 - nX_1^2 - lX_2 X_1^2}{1 + bX_1 + cX_2 + dX_1^2 - bX_1 X_2 + eX_2 X_1^2}, \quad (1)$$

$$l = r_{01v},$$

$$m = r_{12v} (1 + r_{01v}^2),$$

$$n = -r_{01v} r_{12v}^2,$$

$$b = 2r_{01v} r_{12v}, \quad (2)$$

$$c = -r_{12v}^2,$$

$$d = r_{01v}^2 r_{12v}^2,$$

$$e = -r_{01v}^2. \quad (3)$$

In Eq. (1) $X_1$ and $X_2$ are complex exponential functions of film thickness given by

$$X_i = \exp(-j\pi Z_i \cos \phi_i), \quad (4)$$

where $Z_i$ is the thickness of the $i$th film ($i = 1, 2$) normalized to the quarter-wave thickness at normal incidence, i.e.,

$$Z_i = \frac{4d_i n_i}{\lambda}. \quad (5)$$

In Eq. (4) $\phi_i$ is the angle of refraction in the $i$th layer, and in Eq. (5) $n_i$, $d_i$ are the refractive index and metric thickness of the $i$th layer, respectively, and $\lambda$ is the vacuum wavelength of light.

The Fresnel complex-amplitude reflection coefficients of the $ij$ interface for the $p$ and $s$ polarizations are given by[11]

$$r_{ijp} = \frac{n_j \cos \phi_i - n_i \cos \phi_j}{n_j \cos \phi_i + n_i \cos \phi_j}, \quad r_{ijs} = \frac{n_i \cos \phi_i - n_j \cos \phi_j}{n_i \cos \phi_i + n_j \cos \phi_j}. \quad (6)$$

To suppress the $v$ polarization on reflection, we set

$$r_v = 0 \quad (7)$$

in Eq. (1). This gives us the following constraint between $X_1$ and $X_2$:

$$X_2 = \frac{l + mX_1 - nX_1^2}{-n + mX_1 + lX_1^2}. \quad (8)$$

When the refractive indices and angle of incidence are such that $n_1/n_0 < \sin \phi_0$, FTIR takes place at the 01 interface at $\phi_0$ and the light field becomes evanescent in medium 1 (the low-index film). In this case $\cos \phi_1$ is pure imaginary, and $X_1$ is real in the range $0 \le X_1 \le 1$. Because we also choose $n_2 \ge n_0$, the angle of refraction $\phi_2$ in the middle layer is real, which makes $X_2$ a pure phase factor, so that $|X_2| = 1$. For each real value of $X_1$ in the range $0 \le X_1 \le 1$, we find that $|X_2| = 1$ by using Eq. (8). (An analytical proof of this statement is given in Appendix A.) Therefore there is an infinite number of solutions $(X_1, X_2)$ that satisfy Eq. (8) so that $r_v = 0$. The corresponding solution sets of normalized film thicknesses $(Z_1, Z_2)$ are determined subsequently by using Eq. (4).

An acceptable design must have a reflectance

$$R_{v'} = |r_{v'}|^2 \quad (9)$$

for the orthogonal polarization $v'$ that is as close as possible to 1. In general this reflectance increases as the normalized thickness $Z_1$ (of the low-index layers that support the evanescent field) and the angle of incidence $\phi_0$ are increased.
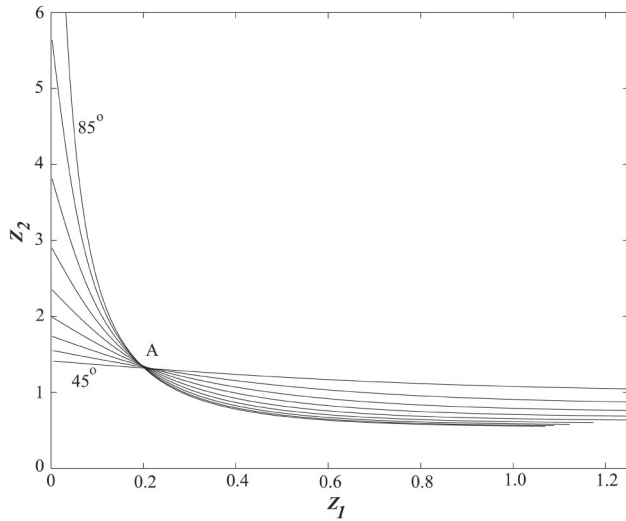
Fig. 2. Plot of $Z_2$ as a function of $Z_1$ such that $r_p = 0$ at angles of incidence $\phi_0$ from 45° to 85° in steps of 5°. We assume MgF$_2$–ZnS–MgF$_2$ trilayers embedded in a ZnS substrate with refractive indices $n_0 = 2.35$ (ZnS), $n_1 = 1.38$ (MgF$_2$), and $n_2 = 2.35$ (ZnS) in the visible spectrum. Notice that all curves appear to have a common point of intersection at A.



Fig. 4. Magnified view of the region of high reflectance in Fig. 3.

## 3. MgF$_2$–ZnS–MgF$_2$ Trilayer Polarizers for the Visible Spectrum

Figure 2 shows $Z_2$ as a function of $Z_1$ such that $r_p = 0$ at angles of incidence $\phi_0$ from 45° to 85° in steps of 5° for MgF$_2$–ZnS–MgF$_2$ trilayers embedded in a ZnS substrate with refractive indices $n_0 = 2.35$ (ZnS), $n_1 = 1.38$ (MgF$_2$), and $n_2 = 2.35$ (ZnS) in the visible spectrum.

In Fig. 3 the associated reflectance $R_s = |r_s|^2$ for the $s$ polarization is plotted versus $Z_1$ at the same angles of incidence as in Fig. 2. It is apparent that $R_s$ increases monontonically with $Z_1$ at a given $\phi_0$ and with $\phi_0$ at a given $Z_1$. Figure 4 shows a magnified view of the region of high reflectance in Fig. 3. Effi-

cient polarizers ($R_s > 99\%$) are readily obtained by using many combinations of $Z_1$ and $\phi_0$.

An interesting feature in Fig. 2 is that all the curves appear to pass through one common point A. If this were true, it would signify that one multilayer can force $r_p = 0$ at many angles of incidence simultaneously. However, as Fig. 5 shows, there is not strictly one common point of intersection for all the curves in Fig. 2. Furthermore, because $Z_1$ at A is small ($\approx 0.2$), the reflectance $R_s$ of such a wide-angle polarizer is low except at high incidence angles, as is evident from Fig. 3.

We now consider the other class of $r_s = 0$ polarizers by using the same MgF$_2$–ZnS–MgF$_2$ trilayer embedded in a ZnS substrate.

Figure 6 shows $Z_2$ as a function of $Z_1$ such that $r_s = 0$ at angles of incidence $\phi_0$ from 45° to 85° in steps of 5°. In Fig. 7 the corresponding reflectance $R_p = |r_p|^2$ for the $p$ polarization is plotted versus $Z_1$ at the
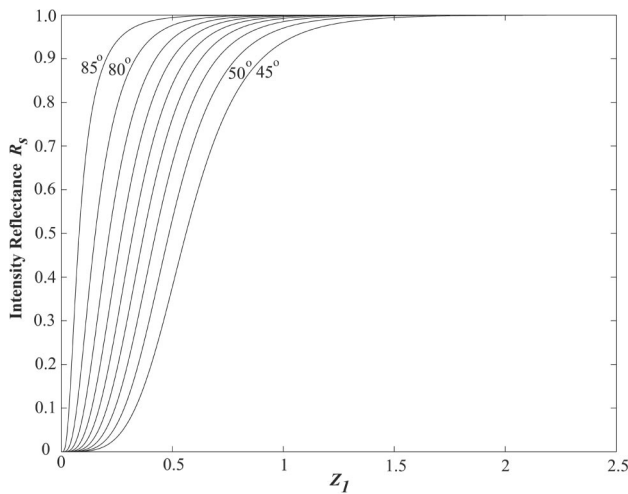


Fig. 3. Reflectance $R_s = |r_s|^2$ for the $s$ polarization is plotted versus $Z_1$ at the same angles of incidence as in Fig. 2 and under the $r_p = 0$ condition.
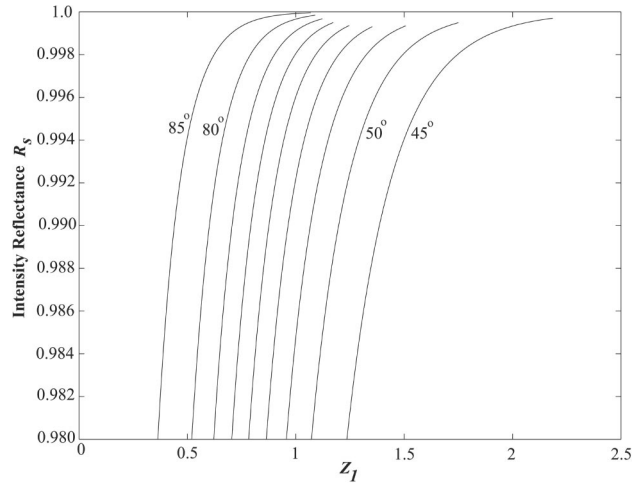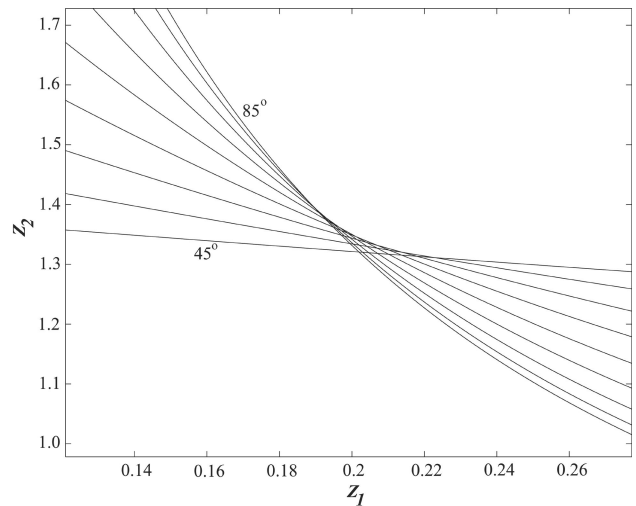


Fig. 5. High-resolution view of the family of curves of Fig. 2 near point A shows that there is not strictly one common point of intersection for all the curves.
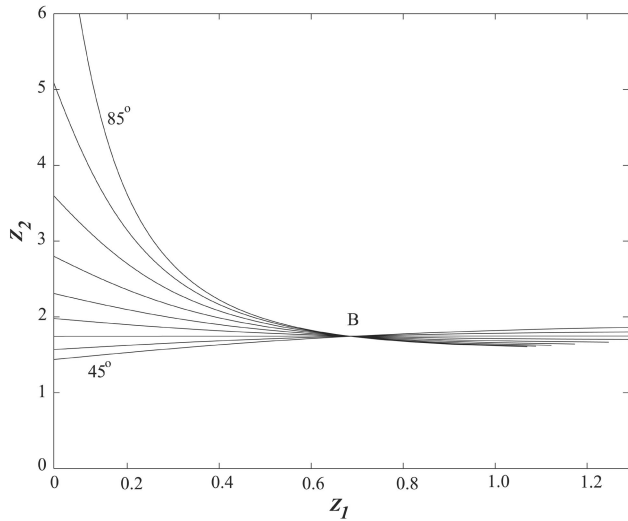
Fig. 6. Plot of $Z_2$ as a function of $Z_1$ such that $r_s = 0$ at angles of incidence $\phi_0$ from 45° to 85° in steps of 5°. All the curves appear to pass through a common point B.

same angles of incidence. Again we find that $R_p$ increases monontonically with $Z_1$ at a given $\phi_0$ and with $\phi_0$ at a given $Z_1$, as one may intuitively expect.

Efficient polarizers with high ER in transmission ($R_p > 99\%$) are realizable by using many combinations of $Z_1$ and $\phi_0$, as is shown more clearly in Fig. 8.

In Fig. 6 all the curves appear to pass through a common point B. Although this is not strictly true, as is shown in Fig. 9, it still suggests that one and the same multilayer can satisfy the condition $r_s = 0$ accurately (although not exactly) at many angles of incidence simultaneously. The value of $Z_1$ at B is large enough ($\approx 0.7$) to make the reflectance $R_p > 90\%$ at all angles $\geq 50°$, as one can see from Fig. 7. This important wide-angle polarizer is considered further in Section 4.
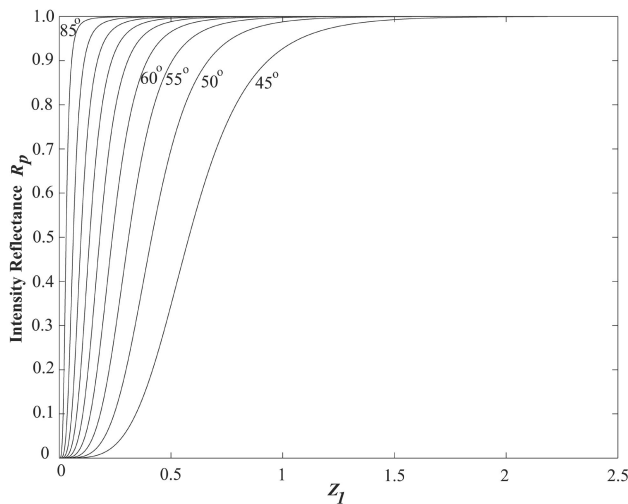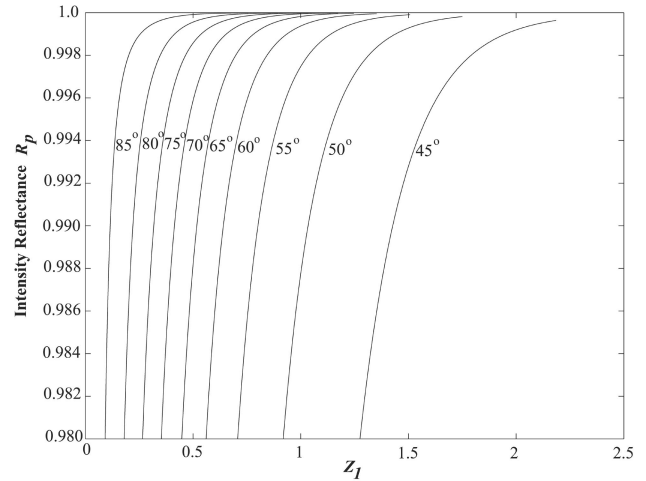


Fig. 8. Expanded view of Fig. 7 in the region of high reflectance.

## 4. Wide-Angle Polarizer Design

This specific design is based on operation at the point of intersection ($Z_1 = 0.6831$, $Z_2 = 1.7472$) of the two curves in Fig. 6 that correspond to $\phi_0 = 55°$ and 75°. The corresponding metric thicknesses of the MgF$_2$ and ZnS films, calculated at a wavelength $\lambda = 633$ nm, are $d_1 = 78.305$ nm and $d_2 = 117.618$ nm, respectively.

Figure 10 shows the reflectances $R_p$ and $R_s$ as functions of the angle of incidence $\phi_0$ from 40° to 85° when the metric film thicknesses and wavelength are kept constant. Note that $R_s < 0.002$ over this entire range of angles and that $R_p > 90\%$ for $\phi_0 > 52°$.

In Fig. 11 the extinction ratios in reflection and transmission (ER$_r$ and ER$_t$ in decibels) are plotted versus the angle of incidence $\phi_0$ from 50° to 80°. Good polarization properties (ER$_r > 40$ dB and ER$_t > 20$ dB) are achieved over an extended range of angles. If one accounts for the refraction of light from air to the



Fig. 7. Reflectance $R_p = |r_p|^2$ for the $p$ polarization is plotted versus $Z_1$ at the same angles of incidence as in Fig. 6 and under the $r_s = 0$ condition.
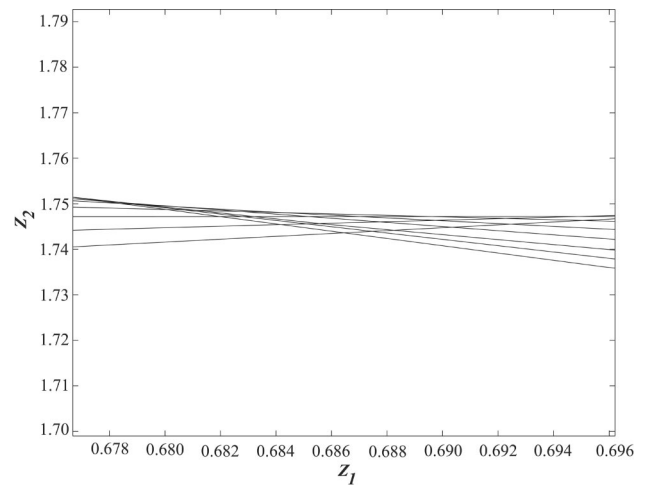


Fig. 9. Magnified view of the family of curves of Fig. 6 in the neighborhood of point B shows that there is not strictly one common point of intersection for all the curves.
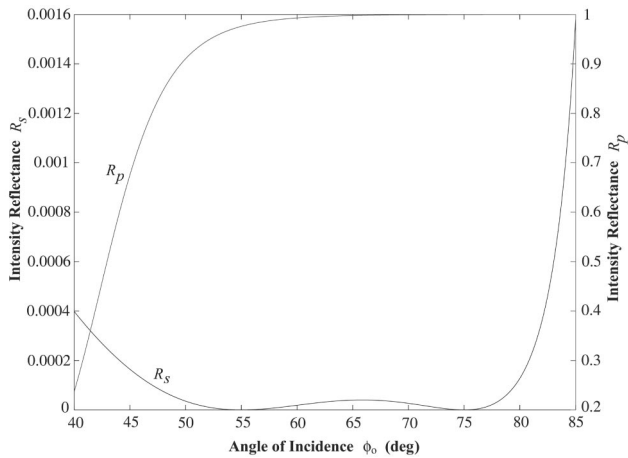
Fig. 10. Reflectances $R_p$ and $R_s$ as functions of the angle of incidence $\phi_0$ from 40° to 85° for a polarizer using a $MgF_2$–ZnS–$MgF_2$ trilayer embedded in a ZnS substrate with refractive indices $n_0 = 2.35$ (ZnS), $n_1 = 1.38$ ($MgF_2$), and $n_2 = 2.35$ (ZnS). The metric film thicknesses ($d_1 = 78.31$ nm, $d_2 = 117.62$ nm) and wavelength (633 nm) are kept constant.
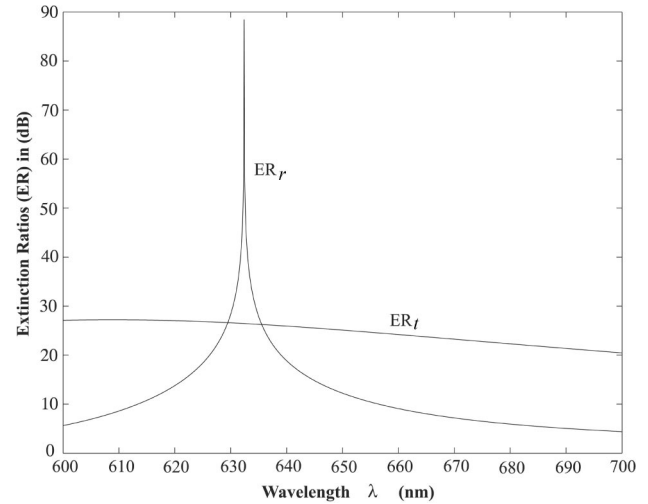


Fig. 12. Extinction ratios $ER_r$ and $ER_t$ in decibels as functions of wavelength $\lambda$ for the wide-angle polarizer of Fig. 10. The metric film thicknesses ($d_1 = 78.31$ nm, $d_2 = 117.62$ nm) and angle of incidence $\phi_0$ (65°) are kept constant.

high-index ZnS substrate, the angular bandwidth in air is even larger that that indicated by Fig. 11.

Although this wide-angle polarizer is intended for use with monochromatic (633 nm) light, it is of interest to consider its performance over a range of wavelengths. For this purpose, the metric film thicknesses $d_1 = 78.305$ nm and $d_2 = 117.618$ nm and the angle of incidence $\phi_0 = 65°$ are kept constant, and the wavelength $\lambda$ is scanned over the 600–700 nm range. In this calculation the dispersion of $MgF_2$ and ZnS over this limited spectral range is ignored. Figure 12 shows the extinction ratios $ER_r$ and $ER_t$ in decibels as functions of $\lambda$. Note that $ER_t$ remains greater than 20 dB over this 100 nm bandwidth, whereas $ER_r$ is high only in the immediate neighborhood of the design wavelength (633 nm).
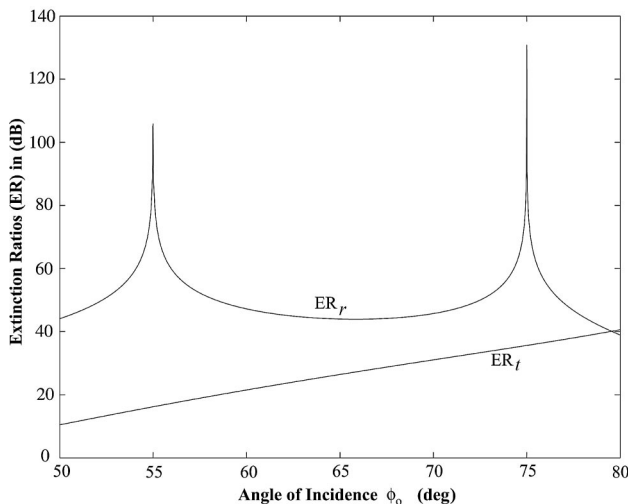
## 5. CaF₂–Ge–CaF₂ Trilayer Infrared Polarizers

Figure 13 shows the constraint between $Z_2$ and $Z_1$ such that $r_p = 0$ at angles of incidence $\phi_0$ from 45° to 85° in 5° steps for $CaF_2$–Ge–$CaF_2$ trilayers embedded in a ZnS substrate with refractive indices $n_0 = 2.2$ (ZnS), $n_1 = 1.4$ ($CaF_2$), and $n_2 = 4$ (Ge) in the infrared. The family of curves in Fig. 13 is substantially different from that of Fig. 2 for the $MgF_2$–ZnS–$MgF_2$ trilayer polarizers in the visible spectrum under the same $r_p = 0$ condition, and a common (or near-common) point of intersection among all the curves does not exist. This significant change is due mostly to the substantially higher refractive index of the center layer (Ge, $n_2 = 4$).
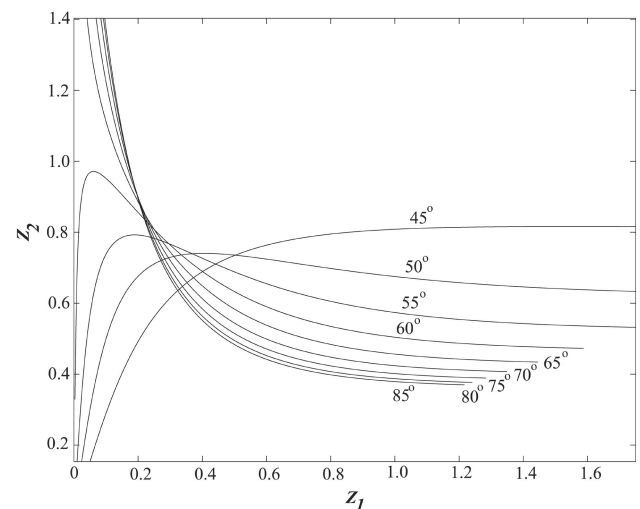
Figure 14 shows the associated reflectance $R_s =$



Fig. 11. Extinction ratios in reflection and transmission ($ER_r$ and $ER_t$) in decibels are plotted versus the angle of incidence $\phi_0$ from 50° to 80° for the wide-angle polarizer of Fig. 10.



Fig. 13. Constraint between $Z_2$ and $Z_1$ such that $r_p = 0$ at angles of incidence $\phi_0$ from 45° to 85° in 5° steps for $CaF_2$–Ge–$CaF_2$ trilayers embedded in a ZnS substrate with refractive indices $n_0 = 2.2$ (ZnS), $n_1 = 1.4$ ($CaF_2$), and $n_2 = 4$ (Ge) in the infrared.
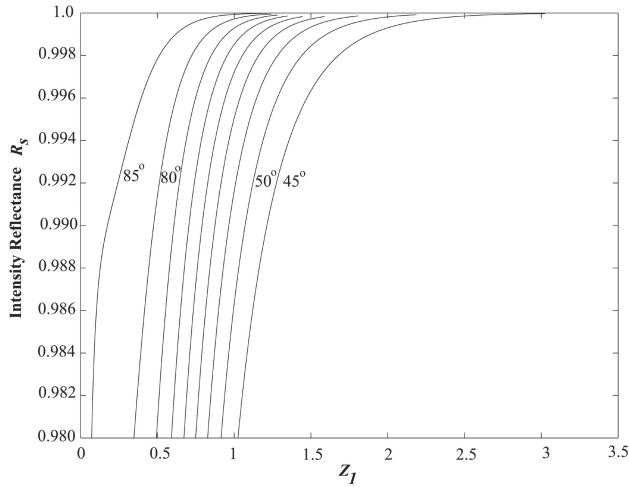
Fig. 14. Reflectance $R_s = |r_s|^2$ for the $s$ polarization plotted versus $Z_1$ under the $r_p = 0$ condition and at the same angles of incidence as in Fig. 13.



Fig. 16. Reflectance $R_p = |r_p|^2$ for the $p$ polarization plotted versus $Z_1$ under the $r_s = 0$ condition and at the same angles of incidence as in Fig. 15.

$|r_s|^2$ for the $s$ polarization plotted versus $Z_1$ at the same angles of incidence as in Fig. 13. Again, $R_s$ increases monontonically with $Z_1$ at a given $\phi_0$ and with $\phi_0$ at a given $Z_1$. Efficient polarizers ($R_s > 99\%$) are readily obtained for many combinations of $Z_1$ and $\phi_0$.

Figure 15 shows $Z_2$ versus $Z_1$ such that $r_s = 0$ at angles of incidence $\phi_0$ from 45° to 85° in 5° steps for the same CaF$_2$–Ge–CaF$_2$ trilayers embedded in ZnS substrate in the infrared. All the curves in Fig. 15 appear to share a common point of intersection C. The associated reflectance $R_p = |r_p|^2$ for the $p$ polarization is plotted versus $Z_1$ at the same angles as in Fig. 16. A wide-angle infrared polarizer that is based on operation at point C of Fig. 15 is possible, and its performance is comparable with that of the visible polarizer discussed in Section 4.
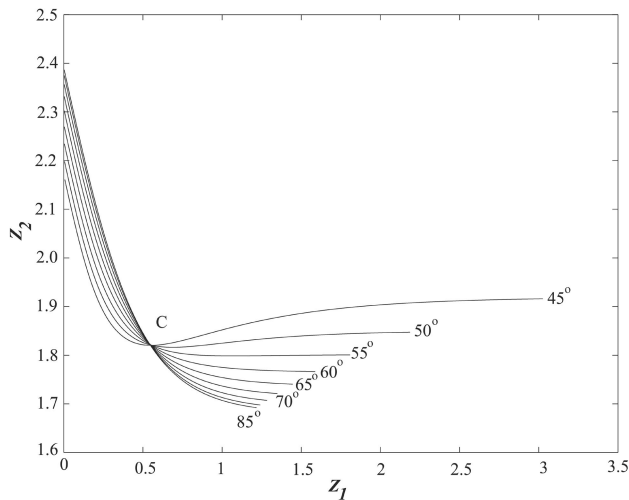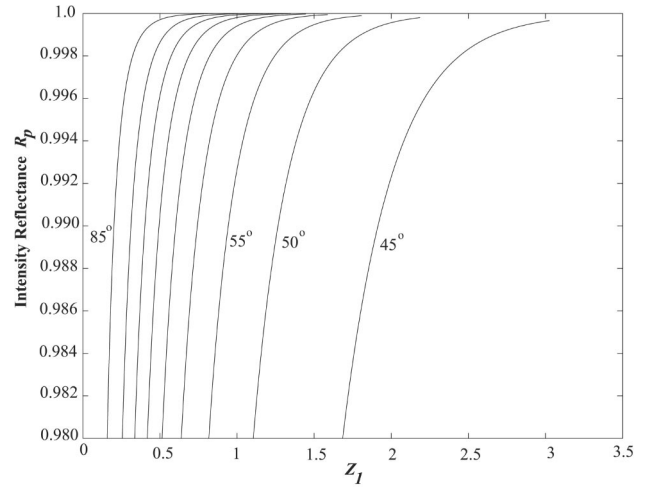


Fig. 15. Plot of $Z_2$ versus $Z_1$ such that $r_s = 0$ at angles of incidence $\phi_0$ from 45° to 85° in 5° steps for CaF$_2$–Ge–CaF$_2$ trilayers embedded in ZnS substrate in the infrared. All the curves appear to share a common point of intersection at C.

## 6. Summary

The polarizing properties of a symmetric trilayer stack embedded in a high-index prism are thoroughly examined by using analytical and numerical calculations. All possible solutions (infinite in number) that suppress the $p$ or $s$ polarization in reflection are determined, and the associated throughput for the orthogonal polarization is calculated. Conditions for obtaining wide-angle designs are clearly demonstrated.

Presented are specific examples of polarizers for the visible spectrum that use MgF$_2$–ZnS–MgF$_2$ trilayers embedded in a ZnS prism to achieve extinction ratios greater than 40 dB in reflection and greater than 20 dB in transmission over a wide range of incidence angles. Infrared polarizers that use CaF$_2$–Ge–CaF$_2$ trilayers embedded in a ZnS prism are also considered.

### Appendix A

In this Appendix we prove that, for each real value of $X_1$ in the range $0 \leq X_1 \leq 1$, $X_2$ as given by Eq. (8) is a pure phase factor; hence $|X_2| = 1$. To do this we substitute $l$, $m$, and $n$ from Eqs. (2) into Eq. (8) and cast the result in the following form:

$$X_2 = \left(r_{12}^2\right) \frac{r_{12}^{-2} + r_{12}^{-1}\left(r_{01}^{-1} + r_{01}\right)X_1 + X_1^2}{r_{12}^2 + r_{12}\left(r_{01}^{-1} + r_{01}\right)X_1 + X_1^2}. \quad \text{(A1)}$$

Under conditions of FTIR, all interface reflection coefficients are pure phase factors; hence

$$r_{ij} = \exp(j\delta_{ij}),$$

$$r_{ij}^{-1} = r_{ij}^* = \exp(-j\delta_{ij}),$$

$$r_{ij}^{-1} + r_{ij} = 2\cos(\delta_{ij}), \quad \text{(A2)}$$

where $\delta_{ij}$ is the interface reflection phase shift.[12] Equations (A2), and the fact that $X_1$ is real, allow Eq. (A1) to be written as

$$X_2 = (r_{12}{}^2)(W/W^*). \qquad (A3)$$

Because each of the bracketed terms in Eq. (A3) is a pure phase factor, it follows that

$$|X_2| = 1. \qquad (A4)$$

For simplicity the polarization subscript $\nu$ was dropped in Eqs. (A1)–(A3).

### References

1. H. A. Macleod, *Thin Film Optical Filters,* 2nd ed. (McGraw-Hill, 1986).
2. A. Thelen, *Design of Optical Interference Coatings* (McGraw-Hill, 1988).
3. J. A. Dobrowolski, "Optical properties of films and coatings," in *Handbook of Optics,* Vol. I, M. Bass, E. W. van Stryland, D. R. Williams, and W. L. Wolfe, eds. (McGraw-Hill, 1995).
4. J. M. Bennett, "Polarizers," in *Handbook of Optics,* Vol. II, M. Bass, E. W. van Stryland, D. R. Williams, and W. L. Wolfe, eds. (McGraw-Hill, 1995).
5. L. Li and J. A. Dobrowolski, "High-performance thin-film polarizing beam splitter operating at angles greater than the critical angle," Appl. Opt. **39,** 2754–2771 (2000).
6. S. M. MacNeille, "Beam splitter," U.S. patent 2,403,731 (6 July 1946).
7. M. Banning, "Practical methods of making and using multilayer filters," J. Opt. Soc. Am. **37,** 792–797 (1947).
8. L. I. Epstein, "The design of optical filters," J. Opt. Soc. Am. **42,** 806–810 (1952).
9. M. C. Ohmer, "Design of three-layer equivalent films," J. Opt. Soc. Am. **68,** 137–139 (1978).
10. CVD, Inc., 35 Industrial Parkway, Woburn, Mass. 01801.
11. R. M. A. Azzam and N. M. Bashara, *Ellipsometry and Polarized Light* (North-Holland, 1987).
12. R. M. A. Azzam, "Phase shifts that accompany total internal reflection at a dielectric–dielectric interface," J. Opt. Soc. Am. A **21,** 1559–1563 (2004).